Systematic Fuel Cavity Asymmetries in Directly Driven Inertial Confinement Fusion Implosions

R. C. Shah,[1,*] B. M. Haines,[1] F. J. Wysocki,[1] J. F. Benage,[2] J. A. Fooks,[3] V. Glebov,[4] P. Hakel,[1] M. Hoppe,[3] I. V. Igumenshchev,[4] G. Kagan,[1] R. C. Mancini,[5] F. J. Marshall,[4] D. T. Michel,[4] T. J. Murphy,[1] M. E. Schoff,[3] K. Silverstein,[4,†] C. Stoeckl,[4] and B. Yaakobi[4]

[1]*Los Alamos National Laboratory, Los Alamos, New Mexico 87545, USA*
[2]*Sandia National Laboratories, Albuquerque, New Mexico 87123, USA*
[3]*General Atomics, San Diego, California 92121, USA*
[4]*Laboratory for Laser Energetics, University of Rochester, Rochester, New York 14623, USA*
[5]*Department of Physics, University of Nevada, Reno, Nevada 89557, USA*

(Received 23 June 2016; revised manuscript received 17 January 2017; published 30 March 2017)

We present narrow-band self-emission x-ray images from a titanium tracer layer placed at the fuel-shell interface in 60-laser-beam implosion experiments at the OMEGA facility. The images are acquired during deceleration with inferred convergences of ~9–14. Novel here is that a systematically observed asymmetry of the emission is linked, using full sphere 3D implosion modeling, to performance-limiting low mode asymmetry of the drive.

DOI: 10.1103/PhysRevLett.118.135001

In the field of inertial confinement fusion (ICF), MJ scale lasers, such as the National Ignition Facility (NIF) [1], are being investigated as a path to create self-sustained fusion burn of hydrogen plasma. A small spherical target containing the hydrogen is imploded, with an important objective being that the drive pressure is amplified so as to satisfy the conditions for self-heating. The direct-drive (DD) approach, in which the laser directly ablates the capsule, is being developed using experiments at the 30 kJ OMEGA facility [2]. An obstacle for the DD path to ignition is that the subscale OMEGA experiments saturate at a pressure twofold below the minimum required for ignition, if scaled for the NIF [3]. Long-wavelength asymmetries have been postulated as the cause, but their role has been inferred on the basis of spatially integrated measurements [4]. In this Letter we present a study of directly laser-driven ICF implosions in which we have used x-ray self-emission of a tracer to visualize, with specificity, the asymmetry of the fuel cavity. By virtue of the technique asymmetry of shape is discovered which suggests that systematic, i.e., shot-to-shot repeatable, character of the on-target laser drive is limiting the achievable pressure.

The importance of implosion symmetry relates to the challenging requirements on pressure with limited laser energy [5]. For self-heating to occur a central "hot-spot" region with temperature ~5 keV must have areal density of the plasma $\rho R \sim 0.3$ g/cm^2, where ρ is the hot-spot mass density and R its radius. Higher density, and thus increased pressure P reduces the total energy as $E \sim P^{-2}$. The required pressures far exceed the drive ablation pressure (by a factor of ~1000) and are obtained from the transfer of kinetic energy of imploding high density fuel or shell into the central low-density hot spot. As this imploding shell of mass decelerates, temperature, density, and, consequently, pressure of the hot spot increase. Asymmetries, depending on their mode (often referenced to the spherical harmonic basis), will impact this pressure amplification. Numerical modeling has shown that $\ell \sim 1$ character can rapidly degrade hot-spot pressure due to incomplete stagnation and a decentering of the pressure profile [4,6,7]. In the OMEGA implosion, low modes that impact pressure might result from large target offset [4] or intrinsic aspects of the power balance suggested by x-ray conversion measurements [8]. Numerous published measurements of OMEGA implosions have diagnosed asymmetry of shell areal density and of fuel conditions in nominal implosions through the use of nuclear and x-ray diagnostics [9–12]. Attention has been lacking though with respect to the origin and impact of the low-mode asymmetries.

In this Letter we present direct connections between observed low-mode asymmetries and their inferred impact. The measurements rely on a novel imaging technique, which enhances signatures from variations at the perimeter of the fuel cavity. To do this, a fine Ti-CH tracer layer is selectively placed only at the innermost surface of the ablator [Fig. 1(a)]. As the capsule decelerates, core conditions heat the Ti dopant to ~keV temperatures and it emits into spectral lines originating from He and H-like ions. From the spectrally resolved images of the self-emission we first identify influence of capsule mounting, predicted as a small perturbation on performance. More importantly, a second systematically repeating asymmetry is argued as strong evidence for a drive asymmetry substantially degrading hot-spot pressure. Using full sphere 3D simulations [4], the impact of drive asymmetry inferred from recently updated x-ray conversion measurements [8] is modeled for our

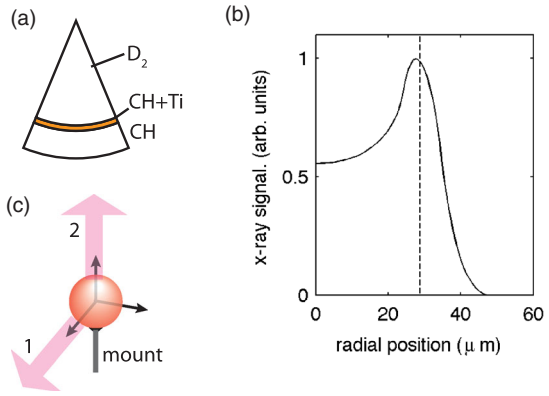

FIG. 1. (a) Self-emission of Ti dopant is used to selectively characterize the shell surface directly in contact with fuel during deceleration. (b) Chord-integrated 5.4–6.0 keV Ti emission from 1D simulation of capsules with initial 0.1 μm thick, 1% by atom Ti tracer layer. The image is calculated for 40 ps gate beginning 100 ps prior to nuclear bang time. Dashed vertical line indicates the position of the fuel-shell interface. (c) Data are presented in the Letter for views both orthogonal and opposite to mounting.

target. The inclusion of the asymmetry accounts for the measured underperformance and, unique to our data set, provides an explanation for the mode 1 signature in the images.

The targets consist of spherical plastic shells with an outer diameter of 875 μm and 20 μm wall thickness which were diffusion filled so as to hold 10 or 15 atm D_2. The innermost 100 nm of the CH is doped with Ti at 1% by atom [Fig 1(a)]. Mandrel characterizations showed low modes ($\ell < 10$) typically at least 2× lower than the inner surface specification used in the ignition campaign at NIF [13]. Maximal variations in wall thickness were nominally 0.1–0.2 μm. Targets were mounted randomly, that is to say without any regard to the orientation of their intrinsic asymmetries.

The targets were imploded in the 60 beam geometry at OMEGA [2] with 23 kJ total energy in a 1 ns square laser pulse. For the data presented, all beams were on target with $\sigma_{\mathrm{rms}} \sim 3\%$ in energy (typical). Standard approaches were employed to minimize single beam nonuniformities, and facility neutron diagnostics provided the basic performance characterizations of neutron yield, Y_n, and burn-weighted-ion-temperature, $\langle T_i \rangle_n$ [14]. Measured Y_n from the D+D→ ^{3}He+n reaction was 30%–40% of calculations assuming 1D behavior, with measured $\langle T_i \rangle_n$ higher than such ideal calculations by 60%.

The choice of laser pulse will determine shell compressibility defined by the ratio of P/P_F, where P_F is the Fermi pressure. Lower values of this quantity, termed adiabat, improve 1D performance but increase susceptibility to hydrodynamic instability [15]. The high-adiabat square pulse was chosen to minimize extraneous physics.

So as to spectrally select for the tracer emission, the images were acquired using an instrument, termed the Multiple Monochromatic Imager (MMI), which combines a pinhole array and a Bragg reflector [16–18]. An advantage of the MMI is that dispersed images can be selectively summed to generate narrow-band images at specific energies. Here we use the band from 5.4–6.0 keV, which encompasses the modest optical thickness He and Ly β emission and results in a composite image averaged over ~20 independent images at each position. The pictures are acquired using a 40 ps gate x-ray framing camera with an additional 15 ps spread due to the different positions along the strip of each photon energy. Figure 1(b) shows the radial variation of the tracer emission from a 1D simulation [19] based on postprocessing using a nonlocal-thermodynamic-equilibrium (NLTE) database of emissivity and opacity for the Ti doped CH [20,21]. Because of the very thin layer, the emission has low optical thickness ($\tau \sim 0.3$), and the contrast of the limb in the chord-integrated emission is primarily determined by the spatial and temporal resolution of the measurement. The limb peaks near the radial coordinate of the doped interface (dashed-vertical line).

In the OMEGA implosions a systematic asymmetry results from the capsule's stalk mounting, which uses a fiber attached to the target with a conical glue fillet [Fig. 2(a)]. In previous simulations (using the 2D DRACO ICF hydrodynamic code [22]) of low-adiabat implosions the presence of the glue fillet was shown to deform the

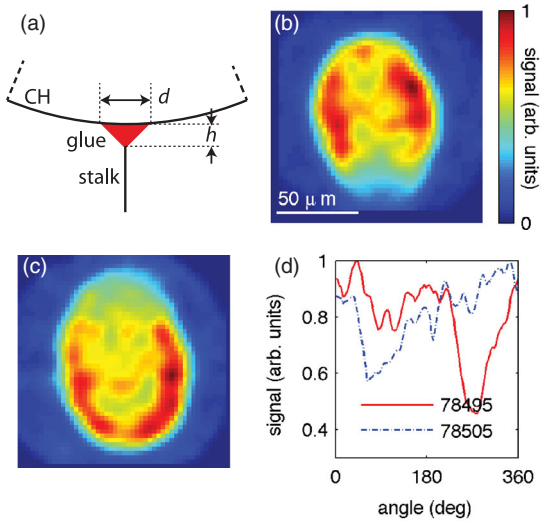

FIG. 2. (a) Omega capsules are positioned at target chamber center using a 17 μm stalk attached to the capsule by a conical glue fillet (typically $d = 80$ and $h = 40$ μm) external to the ablator. (b) Gated Ti self-emission extracted from MMI positioned at view No. 1 [see Fig. 1(c)], with line of sight orthogonal to mounting and mounting from image bottom (shot 78 495). (c) Image from target inserted from diametrically opposite port such that mounting is from image top (78 505). Images are self normalized. (d) Radially integrated signal variation with angle for images of (b) and (c). Angle increases counterclockwise around image center with 0° at the 3 o'clock position. Integration at each angle extends from the 20% intensity contour midway to the image center, and is length normalized.

TABLE I. Yield performance from experiment and 2D simulation for variations of glue fillet dimensions.

Mounting Type	d, h (μm)[a]	Simulation Y_{2D}/Y_{1D} (%)	Experiment[b] Y_{EXP}/Y_{1D} (%)
Nominal	80, 40	...	27 ± 2
Increased	110, 55	79	28 ± 2
Reduced	45, 22	93	29 ± 2
None	0, 0	99	...

[a]see Fig. 2(a); these are nominal values for the target types.
[b]Determined from 3–4 shots for each type; 10 atm DD fill.

inbound shock [23]. This then caused a jetting from the fuel-shell interface with yield degradation specific to the glue parameters. Table I summarizes Y_n from additional DRACO modeling for our implosion over a range of glue parameters and measured yields from experiments (10 atm DD fill). The modeling shows that over this broad parameter range the impact of the asymmetry on yield is modest and varies between ~10%–20%. The experimental yields showed no sensitivity and remained saturated at ~70% below 1D prediction, suggesting other causes dominate the current performance.

The jetting nonetheless results in signatures in our imaged Ti emission. A simple correlation study was made with respect to the mounting position, with the images acquired such that the axis of the mount was perpendicular to the line of sight [view No. 1, Fig. 1(c)]. Figure 2(b) shows an MMI image acquired with the mounting from the view bottom whereas for Fig. 2(c) the mounting was inserted from the port 180° opposite, i.e., image top. The limb brightening anticipated from the 1D simulation is recognizable but modulated, with a prominent feature being reduction of signal from the mount direction. Figure 1(d) shows the azimuthal signal variation of the images. Despite competing asymmetries, the signal minimum is nonetheless observed to correlate with the mount orientations of 270° and 90° (0° at 3 o'clock position in the images). This alignment of signal minimum to mount was typical and showed no obvious change with glue parameters. Mounting, while unlikely to explain our yield degradation, is identified as is the predominant cause of mode 1 character from this view [24].

To place the gated MMI images in the context of the implosion trajectory, we have used a comparison between the averaged radii of the 20% intensity contour and the 1D calculated Ti emission profile. From this analysis, the images of Fig. 2 were determined to be acquired at convergence ratio $C_r \sim 11$ defined by r_i/r_f, where $r_{i,f}$ refers to the initial and final radii of the fuel-shell interface. With respect to the simulated 1D trajectory, this placed the images ~100 ps prior to peak neutron emission, or bang time, and roughly halfway through the deceleration phase.

In a subsequent campaign we collected data from view No. 2 of Fig. 1(c). Here, the imager is directly opposite the capsule mounting, and the mounting is thus not expected to perturb the symmetry of the tracer emission. Figures 3(a), 3(b) show images acquired for two separate shots (15 atm fill, other characteristics as before) with both timed as ~100 ps prior to bang time. The repeatability of the prominent mode 1 in Figs. 3(a) and 3(b) was typical for this data set, and the pattern persisted as the implosion reached bang time, as shown in Fig. 3(c). Averaging three of the later acquisitions, the azimuthal signal variation is ±40% [Fig. 5(a), red-dashed line].

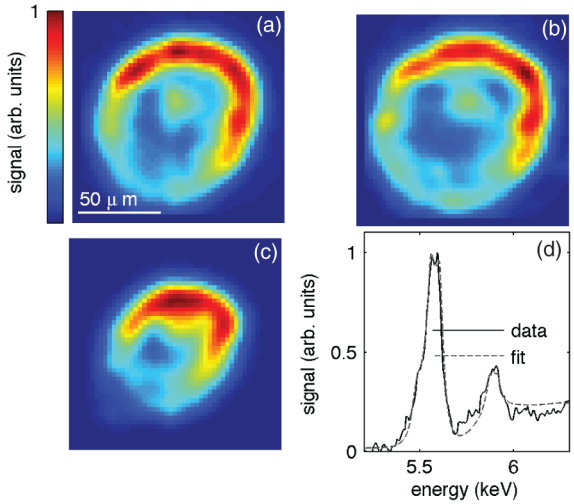

FIG. 3. Data with imager view opposite to capsule mounting, thus minimizing its contribution to observed asymmetry. (a),(b) Ti emission images for shot 79 972 and 79 980, respectively, at ~100 ps prior to bang time. (c) Representative image (79 980) ~100 ps later, i.e., at bang time. (d) Spectrum extracted from MMI gated at bang time with best fit from model ($n_e = 5.5 \times 10^{24}$ e/cm^3 and $T_e = 1350$ eV).

Spectral fitting of the tracer line emission is used to ascertain the emissivity averaged electron temperature T_e and density n_e of the tracer layer. For these near stagnated conditions, the dispersed MMI images were summed to generate a space integrated spectrum [17]. Continuum emission was removed and an exhaustive search was made of n_e, T_e parameter space. The calculated spectra assumed a hollow shell geometry with shell thickness determined from the observed convergence and initial Ti mass. Figure 3(d) shows the continuum corrected experimental spectrum (solid line) and best fit (dashed line) found from 5.4–6.2 keV for $n_e = 5.5$ $[-1.5, +2.5] \times 10^{24}$ e/cm^3 and $T_e = 1.35$ $[-0.35, +0.15]$ keV. In previous experiments of similar implosions at OMEGA, the spatially averaged conditions in the "mantle" or fuel region adjacent to the fuel-shell interface were found to show near 1D performance [25]. Given the uncertainties of our data point, the averaged conditions we have determined might also be considered consistent with values extracted from 1D simulation. However, the images show large variations, or non-1D dependency, in the emission. From the fitted

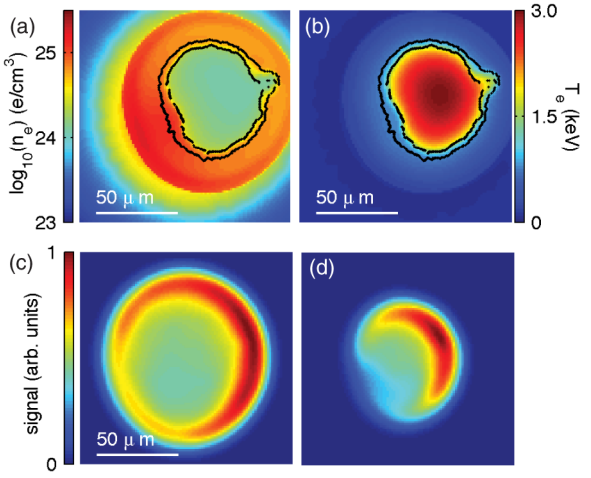

FIG. 4. Results from full sphere 3D simulation with representative beam-to-beam drive asymmetry. (a) A cross-sectional profile of n_e at nuclear bang time with Ti-doped CH regions indicated by black contours. An asymmetry of the density profile aligns to the bulk motion of the target. (b) Corresponding profile of T_e. (c) Calculated 5–6 keV self-emission 80 ps prior to and at (d) bang time.

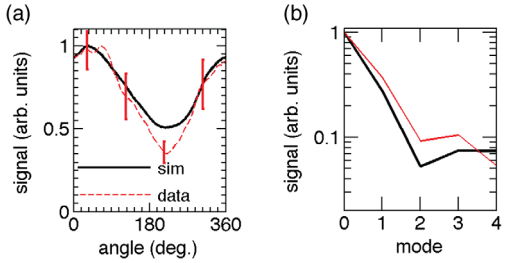

FIG. 5. (a) Comparison of radially integrated emission at bang time between view No. 2 measurements [see Fig. 1(c)] and simulation image [Fig 4(d)]. Signals are phased by aligning their maxima. Error bars on the measurement curve indicate standard deviation obtained from three shots. (b) Fourier series analysis of the signals. Mode 1 amplitude is between 20%–40% of signal and at least 4× greater than other modes for both cases.

parameters we conclude we are not observing threshold behavior of the Ti emission. If the tracer layer is assumed at fixed electron pressure (product n_eT_e remains constant), a ±20% change in temperature or density is needed to account for the signal variation [26].

The observed emission modulation from view No. 2 is linked to drive asymmetry and performance limitations by using the ASTER ICF code [4]. ASTER enables full-sphere 3D simulations, relevant to asymmetries of Legendre modes $\ell \lesssim 10$. Drive asymmetry is captured by using input power, timing, and pointing of each of the 60 beams. At OMEGA, the power histories of the beams are reported for each shot [14]. However, measurements at high power have inferred that the actual on-target intensity does not follow straightforwardly from these values, with the primary impact being to augment the drive $\ell = 1$ [8]. Recent measurements, which indicate the discrepancy persists, have been used to generate a representative drive map for the ASTER simulation, independent of our imaging measurements. Based on a hard-sphere approximation the measurement-corrected drive contains 2% relative amplitude in $\ell = 1$ (quadrature sum over m modes, calculation using VISRAD 3D CAD/view-factor software [27]). As such uncontrolled aspects of the OMEGA system will likely drift over extended periods of time, such a drive map is considered representative only of the magnitude of the low mode asymmetries but not their phasing.

Figures 4(a),4(b) show cross-sectional profiles of n_e and T_e at bang time, in which the black contours indicate the location of the CH-Ti layer. The displacement from center of the profiles indicates a bulk movement due to the $\ell = 1$ in the drive. The tracer layer is at higher density and lower temperature on the overdriven side of the capsule with $\pm \sim 30\%$ low frequency variation in mass averaged conditions. Calculated images with mode 1 character are found over a broad range of observational angles. Examples of synthetic images maximizing mode 1 in emission are shown in Figs. 4(c),4(d) for acquisitions 80 ps prior to, and at bang time. The brighter emission is found to correspond to the higher temperature, lower density regions of the tracer. (Synthetic image calculations indicate a negligible role of opacity.) The evolution of the mode 1 in the emission of the synthetic images qualitatively captures the observations shown in the data of Figs. 3(a)–3(c). In Fig. 5(a) the azimuthal variation of the simulated image at bang time (solid black line) is plotted with the average from experiment (dashed red line). The quantitative levels of mode 1 are comparable [see also modal composition in Fig. 5(b)], thus showing that modeling based on the independent measurements of laser imbalance provides a reasonable explanation for the observations. In the 3D simulation, the burn weighted pressure falls to ~50% of its value from 1D simulation. Y_n is 40% of the 1D value, comparable to the experimental measurement. The much higher experimental $\langle T_i \rangle_n$ of 4.1 keV, as compared to the value of 2.71 keV in the 3D simulation, is consistent with motional broadening of the measurement resulting from $\ell = 1$ asymmetry [4,6].

In conclusion, we have used self-emission from a tracer layer to provide strong, novel evidence for low mode drive asymmetry. This drive asymmetry is identified via modeling as a dominant limit on performance.

We acknowledge Omega staff, T. Sedillo, N. Hoffman, K. Prestridge, B. J. Albright, R. A. Gore, and S. Batha. Support for this work came from the U.S. Department of Energy under Contract No. DE-AC52-06NA25396 (Los Alamos National Laboratory), Award No. DE-NA0001944 (Laboratory for Laser Energetics), the University of Rochester, and the New York State Energy Research and Development Authority.

*rcshah@lanl.gov
†Present address: Department of Physics, Binghamton University, Binghamton, New York 13902, USA.

[1] M. J. Edwards *et al.*, Phys. Plasmas **20**, 070501 (2013).
[2] T. Boehly, D. Brown, R. Craxton, R. Keck, J. Knauer, J. Kelly, T. Kessler, S. Kumpan, S. Loucks, S. Letzring, F. Marshall, R. McCrory, S. Morse, W. Seka, J. Soures, and C. Verdon, Opt. Commun. **133**, 495 (1997).
[3] S. P. Regan *et al.*, Phys. Rev. Lett. **117**, 025001 (2016).
[4] I. V. Igumenshchev, V. N. Goncharov, F. J. Marshall, J. P. Knauer, E. M. Campbell, C. J. Forrest, D. H. Froula, V. Y. Glebov, R. L. McCrory, S. P. Regan, T. C. Sangster, S. Skupsky, and C. Stoeckl, Phys. Plasmas **23**, 052702 (2016).
[5] V. N. Goncharov *et al.*, Phys. Plasmas **21**, 056315 (2014).
[6] B. K. Spears, M. J. Edwards, S. Hatchett, J. Kilkenny, J. Knauer, A. Kritcher, J. Lindl, D. Munro, P. Patel, H. F. Robey, and R. P. J. Town, Phys. Plasmas **21**, 042702 (2014).
[7] B. M. Haines, F. F. Grinstein, and J. R. Fincke, Phys. Rev. E **89**, 053302 (2014).
[8] F. J. Marshall, J. A. Delettrez, R. Epstein, R. Forties, R. L. Keck, J. H. Kelly, P. W. McKenty, S. P. Regan, and L. J. Waxer, Phys. Plasmas **11**, 251 (2004).
[9] V. A. Smalyuk, V. N. Goncharov, J. A. Delettrez, F. J. Marshall, D. D. Meyerhofer, S. P. Regan, and B. Yaakobi, Phys. Rev. Lett. **87**, 155002 (2001).
[10] R. D. Petrasso, J. A. Frenje, C. K. Li, F. H. Séguin, J. R. Rygg, B. E. Schwartz, S. Kurebayashi, P. B. Radha, C. Stoeckl, J. M. Soures, J. Delettrez, V. Y. Glebov, D. D. Meyerhofer, and T. C. Sangster, Phys. Rev. Lett. **90**, 095002 (2003).
[11] H. M. Johns, R. C. Mancini, T. Nagayama, D. C. Mayes, R. Tommasini, V. A. Smalyuk, S. P. Regan, and J. A. Delettrez, Phys. Plasmas **23**, 012709 (2016).
[12] T. Nagayama, Ph. D. thesis, University of Nevada, Reno, 2011.
[13] S. W. Haan *et al.*, Phys. Plasmas **18**, 051001 (2011).
[14] University of Rochester, Laboratory for Laser Energetics, National Laser Users' Facility Users Guide, http://www.lle.rochester.edu/media/omega_facility/documentation/documents/nluf_users_guide.pdf (2007).
[15] P. B. Radha, C. Stoeckl, V. N. Goncharov, J. A. Delettrez, D. H. Edgell, J. A. Frenje, I. V. Igumenshchev, J. P. Knauer, J. A. Marozas, R. L. McCrory, D. D. Meyerhofer, R. D. Petrasso, S. P. Regan, T. C. Sangster, W. Seka, and S. Skupsky, Phys. Plasmas **18**, 012705 (2011).
[16] R. Tommasini, J. Koch, N. Izumi, L. A. Welser, R. C. Mancini, J. Delettrez, S. P. Regan, and V. Smalyuk, Proc. SPIE Int. Soc. Opt. Eng. **6317**, 631716 (2006).
[17] T. Nagayama, R. C. Mancini, R. Florido, R. Tommasini, J. A. Koch, J. A. Delettrez, S. P. Regan, and V. A. Smalyuk, J. Appl. Phys. **109**, 093303 (2011).
[18] B. Yaakobi, F. J. Marshall, and D. K. Bradley, Appl. Opt. **37**, 8074 (1998).
[19] J. J. MacFarlane, I. Golovkin, and P. Woodruff, J. Quant. Spectrosc. Radiat. Transfer **99**, 381 (2006).
[20] C. J. Fontes, J. Colgan, and J. Abdallah, Jr., in *Modern Methods in Collisional-Radiative Modeling of Plasmas*, edited by Y. Ralchenko (Springer, New York, 2016).
[21] C. Fontes, H. Zhang, J. Abdallah, Jr., R. Clark, D. Kilcrease, J. Colgan, R. Cunningham, P. Hakel, N. Magee, and M. Sherrill, J. Phys. B **48**, 144014 (2015).
[22] D. Keller, T. Collins, J. Delettrez, P. McKenty, P. Radha, B. Whiney, and G. A. Moses, Bull. Am. Phys. Soc. **44**, 37 (1999).
[23] I. V. Igumenshchev, F. J. Marshall, J. A. Marozas, V. A. Smalyuk, R. Epstein, V. N. Goncharov, T. J. B. Collins, T. C. Sangster, and S. Skupsky, Phys. Plasmas **16**, 082701 (2009).
[24] In our experiments, the emission is predominantly from implosion periphery. Because of nonuniformities of this emission we are not able to diagnose jetted material above the baseline signal in the chord integration.
[25] S. P. Regan *et al.*, Phys. Plasmas **9**, 1357 (2002).
[26] Emissivity averaging along the line of sight may explain why we do not observe changes in MMI images between the He and Ly β emission lines.
[27] J. J. MacFarlane, J. Quant. Spectrosc. Radiat. Transfer **81**, 287 (2003).